Front. Chem. Sci. Eng. 2024, 18(9): 100
https://doi.org/10.1007/s11705-024-2450-0

RESEARCH ARTICLE

Ultralong hydroxyapatite-based forward osmosis membrane for freshwater generation

Mohamed Gamal Gomaa[1,2], Hamdy Maamoun Abdel-Ghafar (✉)[1], Francesco Galiano[3], Francesca Russo[3], Alberto Figoli[3], El-Sayed Ali Abdel-Aal[1], Abdel-Hakim Taha Kandil[2], Bahaa Ahmed Salah[2]

1 Central Metallurgical Research and Development Institute (CMRDI), 11421 Cairo, Egypt
2 Chemistry Department, Faculty of Science, Helwan University, 11795 Cairo, Egypt
3 Institute on Membrane Technology (CNR-ITM), 87036 Rende, Italy

Abstract Increasing global water shortages are accelerating the pace of membrane manufacturing, which generates many environmentally harmful solvents. Such challenges need a radical rethink of developing innovative membranes that can address freshwater production without generating environmentally harmful solvents. This work utilized the synthesized ultra-long hydroxyapatite (UHA) by the solvothermal method using the green solvent oleic acid in preparing UHA-based forward osmosis membranes. The membranes were developed using different loading ratios of graphene oxide (GO) by vacuum-assisted filtration technique. The prepared GO/UHA membranes were identified using X-ray diffraction, scanning electron microscope, Fourier-transform infrared spectroscopy, and X-ray photoelectron spectroscopy. Water contact angle and pore size distribution were determined for the obtained GO/UHA membranes. The obtained hierarchical porous structure in the prepared membranes with interconnected channels results in a stable water flux with reverse salt flux. The best water flux rate of 42 ± 2 $L \cdot m^{-2} \cdot h^{-1}$ was achieved using the 50 mg GO/UHA membrane, which is 3.3 times higher than the pristine membrane, and a reverse salt flux of 67 $g \cdot m^{-2} \cdot h^{-1}$. The obtained results showed a promising capability of a new generation of sustainable inorganic-based membranes that can be utilized in freshwater generation by energy-efficient techniques such as forward osmosis.

Keywords forward osmosis, ultra-long hydroxyapatite, graphene oxide, inorganic-based membrane

1 Introduction

Polymeric membranes are considered a valid and efficient solution for the separation and purification of wide industrial applications, including desalination, wastewater treatment, gas separation, hemodialysis, and food and beverages industries [1,2]. However, the membrane manufacturing process extensively consumes toxic solvents such as *N*-methyl pyrrolidone, dimethylacetamide, and dimethylformamide for polymer dissolution. These solvents have harmful environmental effects, are expensive, and are considered non-renewable materials [3,4]. To overcome this problem and to catalyze transformation toward a sustainable membrane industry, there are two solutions: the first one through the development of green, non-toxic, and sustainable solvents; and the second one through the synthesis of a new generation of membranes that do not depend on any kind of solvent and could be approached by novel manufacturing processes.

In contrast, inorganic membranes have superior properties in terms of chemical resistance, extended lifetime, good thermal and mechanical stability as well as autoclavability which allow them to be used in harsh conditions like corrosive or hot temperatures [5,6]. Furthermore, the manufacturing process of inorganic membranes does not require the use of toxic solvents. However, inorganic membranes present some drawbacks such as rigidity, fragility, low surface area of the membrane modules, and high capital cost [6,7]. The market of inorganic membranes is still small and growing rapidly with more global attention for developing novel inorganic membranes that could overcome these drawbacks. Hybrid membranes (called mixed matrix membranes) are a new approach to overcome the drawbacks of both polymeric and inorganic membranes combining the benefits stemming from both of them. The

Received January 7, 2024; accepted March 17, 2024; online May 24, 2024

E-mail: hamdy.maamoun@gmail.com

mixed matrix membrane fabrication is based on mixing inorganic nanoparticles with polymer matrixes [8,9].

Recently, promising elongated hydroxyapatite nanowires (ultra-long hydroxyapatite, UHA) were developed by Lu et al. [10]. They proposed a method for the production of UHA nanowires using a precursor of calcium oleate. The synthesized highly flexible UHA nanowires were used to fabricate a novel kind of inorganic paper with excellent thermal and mechanical resistance properties, as well as printing and writing abilities. In addition, several types of functional paper sheets based on UHA nanowires have been developed, with great potential for use in different areas such as biomedicine, sterilization, environmental and food safety [11]. Zhang et al. [12] prepared filter paper nanosheet by reaction of double metal oxide with UHA nanowire for dye removal from wastewater. Qin et al. [13] developed a photothermal hydrogel through the reaction between a composite of carbon nanotubes and UHA to obtain an aerogel with highly efficient solar energy-assisted water purification. This wide range of promising applications that utilize UHA materials makes it highly recommended for many applications due to its unique thermal and mechanical properties with the semi-flexibility of its assembled sheets.

The rapid increase in the scarcity of freshwater due to the accelerating impact of climate change forces the world to respond sustainably [14,15]. Utilizing UHA for assembling membranes for water purification using vacuum assisted filtration technique is considered a sustainable membrane fabrication technique since there is no solvent used in the membrane fabrication and the only solvent used in precursor UHA preparation, oleic acid, is a green solvent. The application of such developed inorganic-based UHA membrane in the forward osmosis (FO) technique will overcome the organic fouling problem and encourage using draw solutions at high temperatures to increase the water flux. FO is an energy-saving water purification method, using an osmotic membrane process with a partially permeable membrane that differs from reversing osmosis by not applying the pressure required to separate dissolved substances such as ions and molecules and larger particulates [16].

Due to its sp2 covalent bonds and electron mobility, graphene has a wide range of important mechanical, thermal, catalytic, physical, and optical properties in many areas of science and engineering [17]. Graphene's exceptional properties include very strong mechanical strength, elasticity, tunable band, and excellent heat and electrical conductivity. The formation of water channels among graphene oxide (GO) layers has been demonstrated, thus indicating high flux in the filtration process, by using GO transparent membranes [18]. In various water treatment areas, including seawater desalination and the recovery of organic solvents, GO-based membranes have been used [19]. It is an efficient way of separating various materials by adjusting the distance between GO layers [19]. It is expected that the GO, two-dimensional (2D), interacts with the UHA nanowires, one-dimensional (1D), forming a three-dimensional (3D) network that will allow water to run out between the formed microchannels and retain the pollutants, leading to the development of highly efficient FO membrane for wastewater treatment.

In this work, we developed inorganic-based FO membranes using UHA nanowires as a base of inorganic materials with 1D structure with other different microstructure materials of GO as 2D structure. The FO membranes were fabricated via a vacuum-assisted filtration technique. The performance evaluation of the developed FO membranes was carried out using the assembled Sterlitech FO system. The water flux and reverse salt flux of the prepared membranes were determined.

2 Experimental

2.1 Chemicals and materials

NaOH (assay 98%–100%), and ethanol absolute (assay ⩾ 99.9%) were obtained from Merck, Germany. H_3PO_4 (assay 85%), H_2O_2 (assay 49%–51%), and H_2SO_4 (assay 96%–98%) were purchased from Dop Organic Kimya, Turkey. HCl (assay 37%) was obtained from Merck, Germany. $CaCl_2$ (assay 95%) and sodium dihydrogen phosphate monohydrate ($NaH_2PO_4{\cdot}H_2O$, assay 98%) were purchased from Adwic, Egypt. Graphite (assay 99.5%) was obtained from Alpha Chemika, India. Oleic acid (assay 65%–70%) was purchased from Central Drug House, India. $KMNO_4$ (assay 99.0%–100.5%), was obtained from NORMAPUR, and fiberglass (commercial product grade) was purchased from an Egyptian local market. All chemicals have been used as they were received without further purification. All experiments were performed using bi-distilled water.

2.2 Synthesis of UHA nanowires

The UHA nanowires were obtained during the calcium oleate major solvothermal method [20,21]. NaOH (10.5 g), $CaCl_2$ (3.33 g), and $NaH_2PO_4{\cdot}H_2O$ (8.4 g) were dissolved in 150.0 mL of bi-distilled water, respectively. These formed aqueous solutions were separately added into a mixture of ethanol (47.5 g), oleic acid (93.6 g), and bi-distilled water (135 mL) with continuous stirring. The resulting suspension was transferred into a 1 L Teflon-lined stainless-steel autoclave that was sealed and heated at 180 °C for 24 h. The autoclave product was separated and washed three times with ethanol and deionized water after cooling to room temperature. The obtained value

was determined after drying at a temperature of 90 °C. The obtained yield was 2.4 g. The synthesis method is explained in Fig. 1.

2.3 Preparation of UHA membrane

In the membrane fabrication, we depend on the known value of the UHA nanowires yield and after ethanol washing, we added the fiberglass and GO to the UHA nanowires suspension and for each autoclave, three membranes were prepared containing each one an amount of UHA nanowires of about 0.8 g. The GO was obtained from graphite by the modified Hummer method as explained in the supplementary [22,23]. Figure 1 illustrates the fabrication process of the highly porous UHA membrane. Specifically, 0.8 g of UHA nanowires was ultrasonicated and mixed very well with 0.133 g of fiberglass. The mixed commercial fiberglass was cut by scissors and washed with water and ethanol, then dried before using it. The GO/UHA membranes were prepared by mixing and ultrasonication the desired amount of GO (0, 10, 20, 30, 40, 50, and 60 mg) with the UHA/fiberglass mixture as previously explained. After that, the obtained suspension was vacuum filtrated with a diameter of 7.0 cm followed by drying manually for 5 min using iron at about 150 °C where the membrane was placed between two fabric layers (Fig. S1, cf. Electronic Supplementary Material, ESM).

2.4 Characterization

The morphology of synthesized UHA nanowires was investigated by the transmission electron microscope (TEM, Hitachi H50, Japan-76). Variable pressure scanning electron microscopy (SEM, Hitachi S3400, Japan) was applied to characterize the surface morphology and cross-sectional microstructure of the fabricated UHA membranes. X-ray photoelectron spectroscopy (XPS, ESCALAB 250Xi, USA), X-ray diffraction (XRD, Cu Kα radiation, k = 1.54178 Å, D/max 2550 V, Rigaku, Japan), and Fourier transform infrared spectra (ATR-FTIR, Nicolet iN10, USA) were used to characterize the prepared UHA membranes through investigating their functional groups and chemical compositions. The membrane surface wettability was tested by using CAM 100 (KSV Instruments, Ltd.) through triplicate measurements of each membrane in different locations. The thickness of UHA membranes was determined by coating thickness gauge PCE-CT 23BT device (PCE Instruments UK Ltd.). Pore size flow distribution was determined using POROLUX^{TM} 1000 (Porometer, Belgium). The surface roughness was measured using an atomic force microscope (Flex AFM).

2.5 Performance evaluation of the UHA membranes

The performance evaluation of the UHA membranes was evaluated using FO laboratory-scale device, as shown in Fig. 2. The feed solution (bi-distilled water) and the draw solution (2.0 mol·L^{-1} NaCl) were circulated with two micropumps (Cole-Parmer, 3.2 LPM). The developed UHA membranes were placed between the feed and draw solutions using Sterlitech FO cell (CF016, PTFE, USA), as explained in Fig. S2 (cf. ESM). Equations (1) and (2) calculated the water flux and reverse salt flux respectively [24,25]. To determine the water flux and reversal salt, an average of at least two pieces of membranes has been measured.

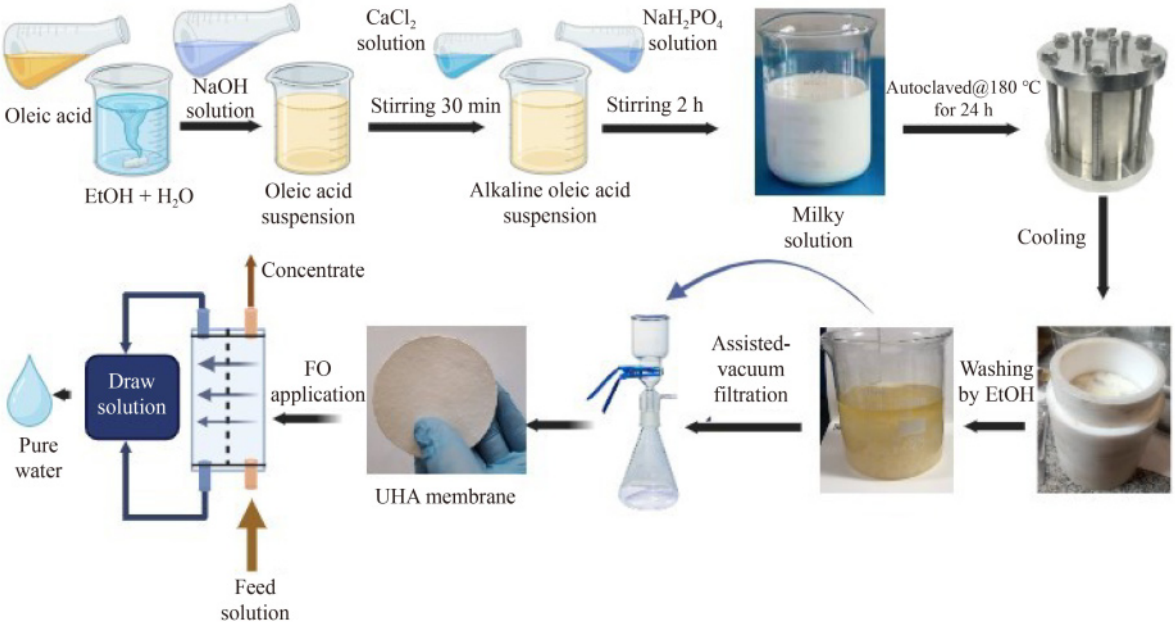

Fig. 1 Preparation of the UHA membrane.

$$J_v = \frac{\Delta m}{A \times \Delta t \times \rho_0}, \quad (1)$$

where J_v ($L \cdot m^{-2} \cdot h^{-1}$, LMH) is the water flux. Δm (g) is the weight change of the feed solution, which was recorded automatically every 1.0 min by an electronic balance (ME3002E, Mettler Toledo) connected to a computer-assisted by EasyDirect^{TM} license key. A (m^2) is the membrane surface area, Δt (h) is the time interval (1.0 min), and ρ_0 is the pure water density (0.997 $g \cdot cm^{-3}$ at room temperature 25 °C).

$$J_s = \frac{(C_t V_t - C_0 V_0)}{A \times \Delta t}, \quad (2)$$

where J_s ($g \cdot m^{-2} \cdot h^{-1}$, gMH) is the reverse salt flux. C_0 and C_t ($g \cdot L^{-1}$) are the initial and final concentrations of the feed solution, respectively, which are detected by a conductivity meter by the MIC meter industrial company. V_0 (L) and V_t (L) are the initial and final volumes of the feed solution, respectively.

The stability of the membrane has been assessed through a continuously running test at mode over an extended duration for more than 100 min. The weight was recorded every minute and conductivity was measured, for the feed solution, at the beginning and the end of the experiment.

3 Results and discussion

3.1 Characterization of the UHA nanowires

Shortly, the UHA nanowires were obtained from NaOH and oleic acid by acid-base reaction. Sodium oleate is used as a reactant, an emulsifier, and a surface modifier in the hydrothermal process. At room temperature, sodium oleate, and $CaCl_2$ react to make calcium oleate (the precursor) that hydrothermally reacts with monosodium phosphate to form monodispersed UHA nanowires.

Because calcium oleate has a modest solubility product constant, it releases calcium cations into the aqueous reaction solution slowly, which causes UHA to nucleate slowly and helps the nanowire shape grow regularly. The UHA nanowires were synthesized through the calcium oleate major solvothermal method. The diameter and length of the as-prepared UHA nanowires are ~20–100 nm and up to several hundred micrometers, respectively [12]. In many cases, the UHA nanowires are self-assembled into nanowire bundles along the longitudinal direction, as shown in Fig. 3.

3.2 Characterization of the UHA-based membranes

Figure 4 shows the fabricated UHA-based membranes (Figs. (a–d)) with a schematic illustration of the UHA and GO interactions (Fig. 4(e)). The UHA nanowires are wrapped and aligned with GO through hydrogen bonding, coordination interaction, or van der Waals forces to form a hierarchical nanocomposite during the membrane assembly process. The UHA-based membranes were prepared by mixing the homogenous dispersed UHA nanowires and GO nanosheets with fiberglass. To enhance the mechanical strength of the membrane, fiberglass is introduced. The mechanical tests of the prepared membrane were performed and achieved Young's Modulus (MPa) of 35 ± 5, and Elongation at break (%) of 38 ± 10. After drying, aqueous suspensions containing UHA nanowires, GO, and fiberglass is filtered under vacuum using a commercial sheet of paper and formed from UHA-based membranes. To enhance the water flux ability for membranes, the GO was added in different concentrations (0, 10, 20, 30, 40, 50, and 60 mg).

3.2.1 SEM analysis

The morphologies of UHA-based membranes were characterized by SEM, as shown in Fig. 5. The membranes of UHA nanowires and fiberglass have a highly porous and nacre-like multilayered cross-sectional structure. The investigated surface morphology of the UHA/GO membranes indicates that UHA nanowires and

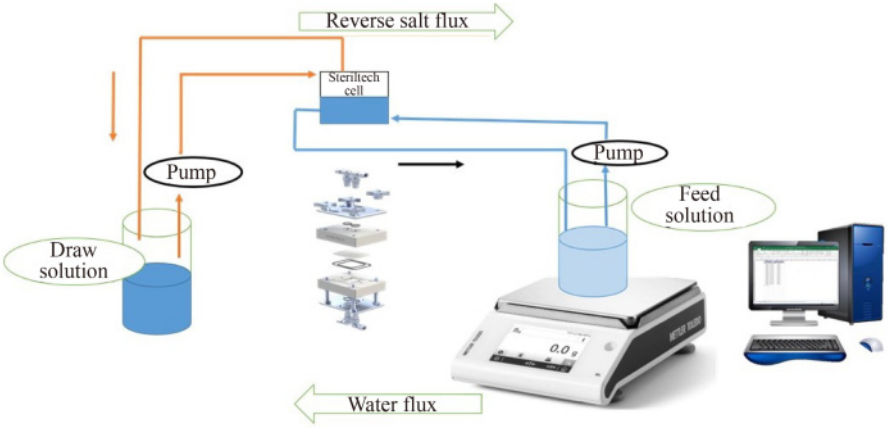

Fig. 2 Schematic illustration of the FO system used to determine the UHA membranes performance evaluation.

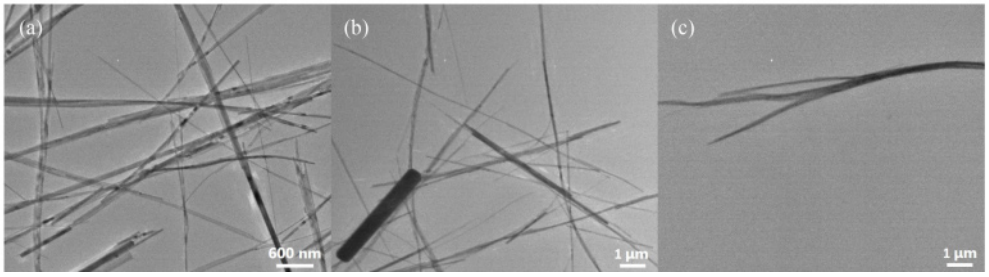

Fig. 3 TEM images of the synthesized UHA nanowires at different magnifications: (a) at 600 nm, and (b, c) at 1.0 µm.

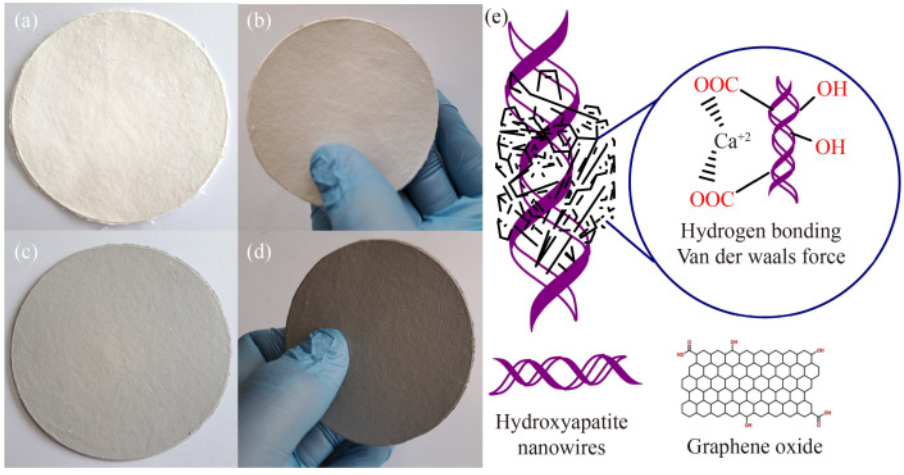

Fig. 4 The prepared UHA-based membranes with different loads of GO: (a) 0 mg, (b) 10 mg, (c) 30 mg, (d) 60 mg, and (e) a schematic illustration of UHA and GO interactions.

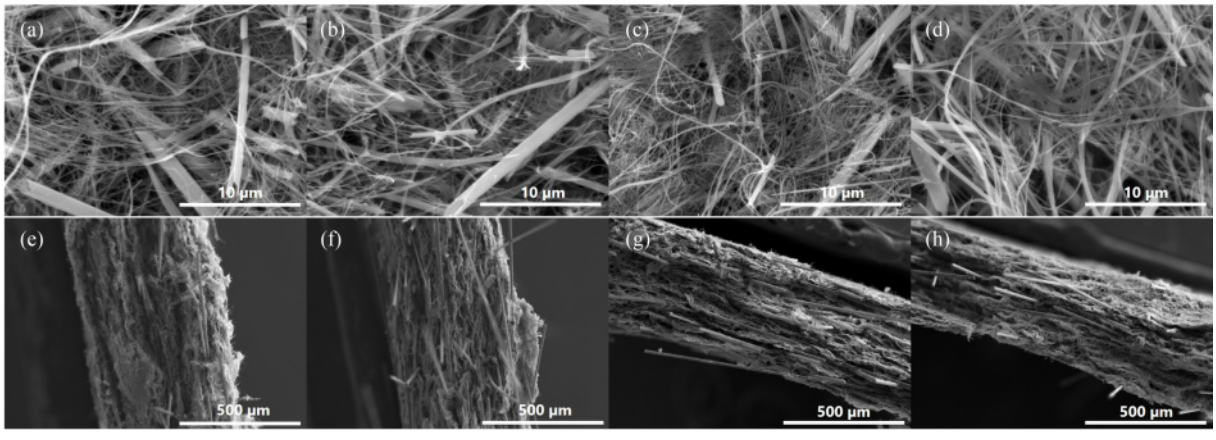

Fig. 5 The SEM morphology analysis for the top layer of the prepared membranes 0, 10, 20, and 30 mg GO/UHA of (a), (b), (c), and (d), respectively. The SEM cross-sectional analysis for the prepared membranes 0, 10, 20, and 30 mg GO/UHA of (e), (f), (g), and (h), respectively.

some pores are covered with carpet-like GO nanosheets, but many pores are still visible and the nacre-like layered structure is visible in top surface morphology analysis (Figs. 5(a–d)) and cross-sectional analysis (Figs. 5(e–h)).

The cross-sectional analysis of the UHA-based membranes of 0, 10, 20, and 30 mg of GO (Figs. 5(e–h)) shows a decrease in membrane thickness from 650 to 410 µm, with increasing the loading ratios of GO from 0 to 30 mg, respectively. The same results were obtained by measuring the membrane thickness using the thickness gauge instrument where the thickness reduced from 690 ± 56 to 341 ± 5 by loading GO from 0 to 60 mg, as shown in Table 1. This thickness reduction is due to the increasing hydrogen bonding between the GO and UHA nanowires that contribute to more ordering for the nacre-like layers structure. The top surface analysis of the fabricated GO/UHA membranes is shown in Fig. S3 (cf. ESM). However, there is no big change in the thickness

of the 30 and 40 mg GO/UHA membranes, and the same for the 50 and 60 mg GO/UHA membranes. This may refer to the low density in the functional groups of GO.

3.2.2 XRD analysis

The XRD spectra of the prepared GO/UHA membranes are shown in Fig. 6. The characteristic peaks of UHA include peaks at 2θ of 26.5°, 28.7°, 31.8°, 32.8°, 40°, 50.5°, 51.3°, 52.1°, and 60°, which is marked in the figure with an asterisk [26]. The characteristic peak of GO appeared in all the prepared GO/UHA membranes except the blank one without GO at $2\theta = 10.6°$ [27]. The XRD of GO is shown in Fig. S4 (cf. ESM). A reduced GO (rGO) characteristic peak appeared at $2\theta = 21.7°$ in all UHA-based membranes doped with GO [27,28]. The appearance of the rGO peak may be attributed to a reduction in the portion of the doped GO in the membranes during the drying method by iron for a few minutes at about 150 °C [29]. So, the prepared UHA-based membranes exhibit a main composition of hydroxyapatite with different ratios of GO and rGO.

3.2.3 Surface wettability

Surface roughness affects the wettability of the membrane and thus the water contact angle as well as adhesion. In general, surface roughness improves wettability at small contact angles (angle becomes smaller), and reduces it at large contact angles (angle becomes larger). The resulting superhydrophobic surface of the developed UHA/GO membranes is due to the rough surface texture of the used materials (UHA nanowire and fiberglass) where their smooth surface is non-wettable, in addition to the low density in the functional groups of GO due to its thermal reduction during the direct membrane drying. The roughness of the prepared membranes was measured by the atomic force microscope and showed high surface roughness with *Sq* vale varied from 45 to 338 nm, as shown in Fig. 7(a).

The prepared UHA-based membranes showed hydrophobic surface characteristics. The water contact angle is a function of the loading ratio of GO and its reduced ratio to rGO due to the drying method by iron at about 150 °C, and the surface roughness of the membrane due to the mixed fibers ratios of UHA nanowires and fiberglass (5.7:1). Figure 7(b) shows that the contact angle of the pristine membrane and the 10 mg GO/UHA membrane are comparable with a value of 136.7°, while the contact angle of the 20 mg GO/UHA membrane decreased to 122.4°. This may be due to the fact that the surface is smoother than other prepared membranes as shown in the SEM results (Fig. S4). The increase in contact angle from 137.7° to 150.3° with the increase in the loading ratio of GO from 30 to 60 mg is attributed to the increased loss of oxygen groups of GO through its conversion into rGO as a consequence of thermal reduction during the membrane drying [29,30]. This rough surface texture leads to capillary depression where the capillary force doesn't pull the liquid inward but pushes it outward. The relationship between the roughness and the water contact angle is explained by Wenzel, and Cassie-Baxter models, as shown in Fig. 7(d) and supplementary file (section S3, cf. ESM).

Table 1 The thickness of the prepared GO/UHA membranes

Membrane	Thickness/μm
0 mg GO/UHA membrane	690 ± 56
10 mg GO/UHA membrane	557 ± 1.0
20 mg GO/UHA membrane	466 ± 10
30 mg GO/UHA membrane	430 ± 29
40 mg GO/UHA membrane	439 ± 5
50 mg GO/UHA membrane	319 ± 10
60 mg GO/UHA membrane	341 ± 5

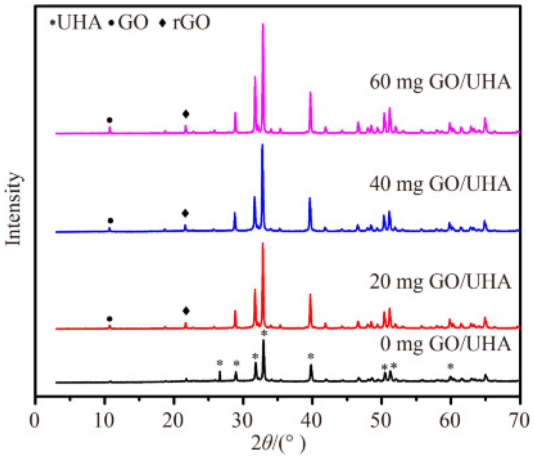

Fig. 6 XRD of the UHA-based membranes.

3.2.4 FTIR analysis

Figure 8 shows the FTIR spectra of the pristine UHA membrane and the GO/UHA membranes. The FTIR spectrum of the pristine UHA membrane shows adsorption peaks at 1126, 1073, 962, and 604 cm^{-1} ascribable to the PO_4^{3-} group, and the adsorption peaks at 3435 and 3573 cm^{-1} originating from the adsorbed water and hydroxyl group, respectively [31]. The characteristic adsorption peaks of both ultralong hydroxyapatite nanowires and GO are observed in the FTIR spectrum of the GO/UHA membranes, and two characteristic absorption peaks at 1718 and 1617 cm^{-1} are attributed to the C=O and aromatic C–C vibrations of GO, respectively (Fig. S5, cf. ESM) [32]. The peaks at 2927 and 2855 cm^{-1} are attributed to the stretching vibration of $–CH_2–$. The peak at 1715 cm^{-1} of oleic acid is derived from the C=O from the –COOH group [33]. When oleic acid reacts with Ca^{2+} ions in an alkaline solution to form calcium oleate,

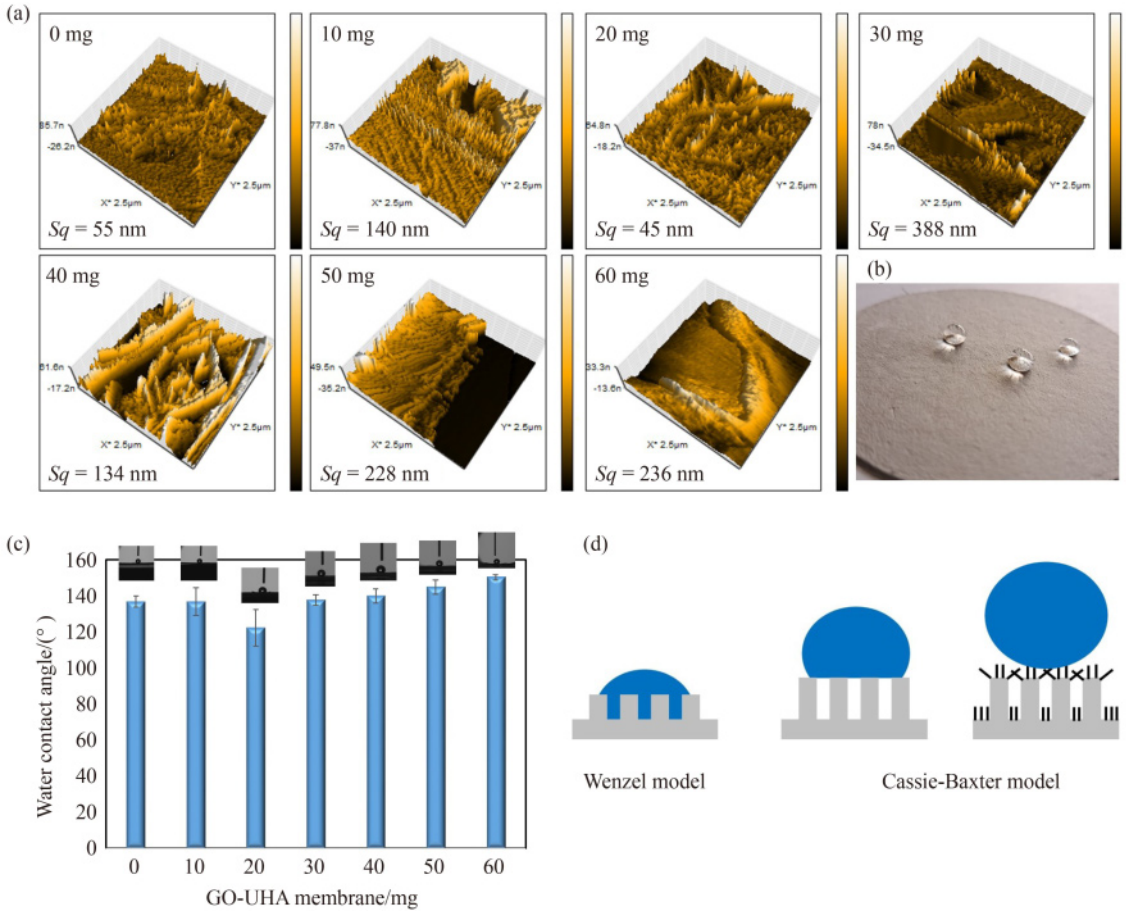

Fig. 7 (a) The AFM images "derived data" of the top surface of GO/UHA membranes, (b) an image of stable water drops on the top surface of 60 mg GO/UHA membranes, (c) water contact angle of the GO/UHA membranes, and (d) a schematic illustration of Wenzel and Cassie-Baxter models.

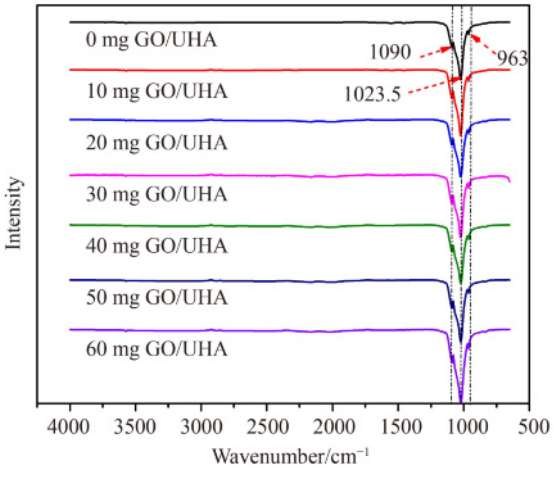

Fig. 8 FTIR analysis of the GO/UHA membranes.

the peak shifts and splits into two peaks at 1581 and 1540 cm^{-1} as shown in detail in Fig. S5 [34].

3.2.5 XPS analysis

The surface composition of the as-prepared GO/UHA membrane was determined by XPS analysis (high-resolution XPS spectra of the Ca 2p, P 2p, C 1s, and O 1s region), as shown in Fig. 9. It displays the Ca 2p high-resolution XPS spectra with two significant peaks corresponding to Ca $2p_{3/2}$ and Ca $2p_{1/2}$, respectively, at 347.9 and 350.5 eV (Figs. 9(b) and 9(c)). The high-resolution XPS spectrum shows a peak at 133.4 eV which corresponds to a phosphate group (P 2p) in the UHA nanowires (Fig. 9(d)). The nanocomposite shown in Fig. 9(e) has a single peak at 285.88 eV (the oxygenated functional group of carbon sp (C–O)) in its C 1s core level XPS spectra. These findings suggest that during the hydrothermal reduction process, GO nanosheet surfaces still contain functional groups. The O 1s XPS spectrum can be deconvoluted into one distinct peak with a binding energy of 532.28 eV. The obtained XPS results (Fig. 9(f)) demonstrate that the UHA nanowires were successfully grown on the surfaces of GO sheets by creating hydrogen bonds and van der Waals force [35–37].

3.2.6 Pore size analysis

The pore size analysis of the fabricated GO/UHA membranes with different loading ratios of GO was

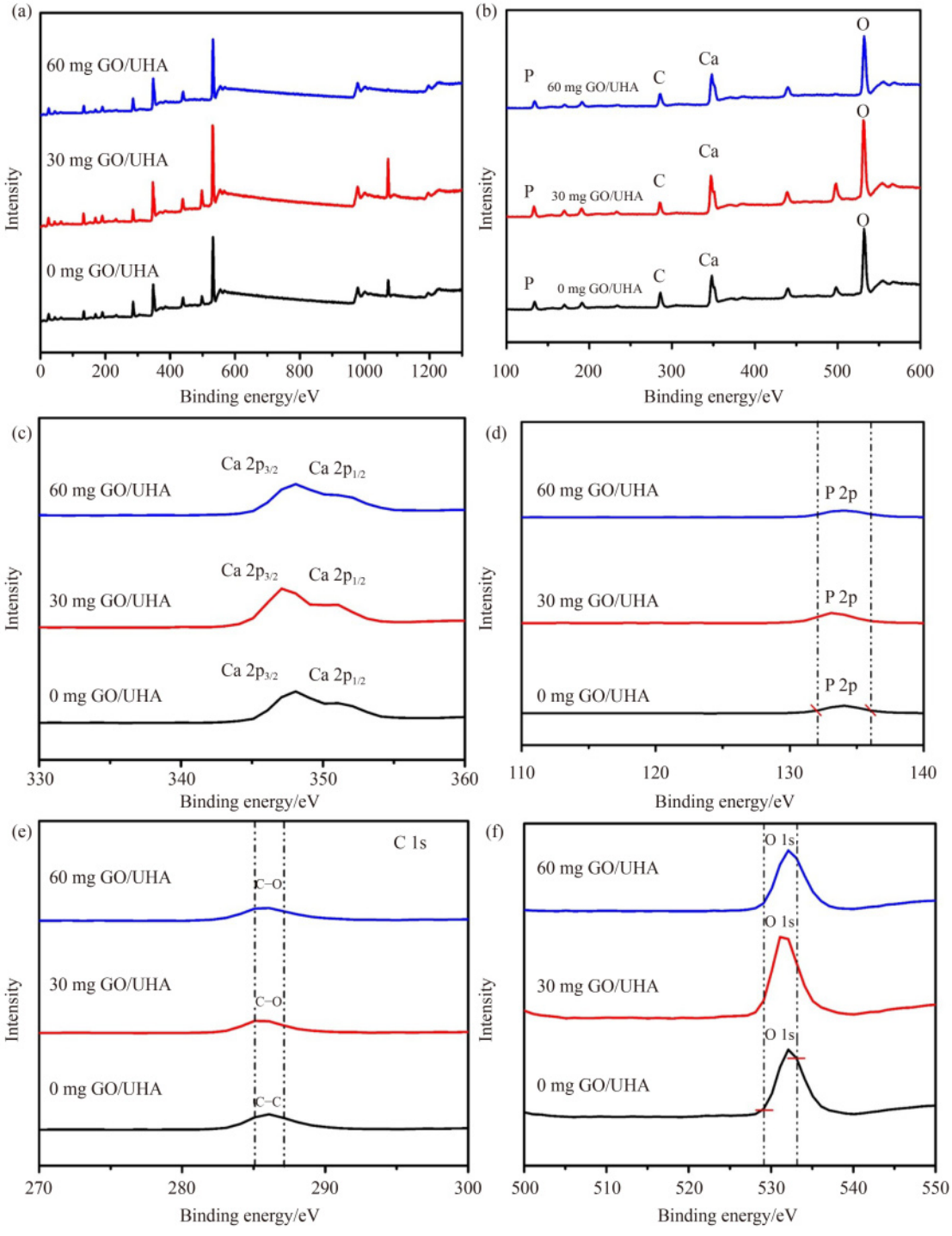

Fig. 9 XPS analysis of the GO/UHA membranes.

explained in detail as shown in Fig. 10. The mean flow pore size (MFP) was increased from 0.44 μm for the pristine UHA membrane to 1.21 μm for the 20 mg GO/UHA membrane (Fig. 10(a)). Generally, the addition of GO with a thermally converted ratio to rGO as previously explained and shown in XRD may lead to low interactions with UHA nanowires resulting to an increase in the pore size of the GO/UHA membranes that ranged from 0.74 μm for the 50 mg GO/UHA membrane to 1.21 μm for the 20 mg GO/UHA membrane. This reflects the higher interactions and hydrogen bonding between GO and UHA. The pore size flow distribution (percent flow) is represented in Fig. 10(b). Compared to other membranes, the 50 mg GO/UHA membrane showed a uniform pore size distribution of three major ratios presenting 75% at 0.59 μm, 13.1% at 0.8 μm, and 8.7% at 0.46 μm. This uniform pore size distribution confirms the high interconnected pores with enhancing water flux.

3.3 Performance evaluation of the UHA-based membranes

The performance of the membranes was evaluated in terms of water flux as shown in Fig. 11. The water flux varied from 8.9 to 42.3 LMH, as shown in Fig. 11(a). The variation in water flux of the prepared UHA-based membranes is a function of loading ratio of GO and the reduced ratio to rGO, the wettability and roughness of the membrane surface, in addition to the thickness of the membrane. The membrane was cut and fixed by a water-proof tap that was placed in the FO cell, after water stability testing (Fig. S6, cf. ESM). The membranes showed excellent mechanical stability in the wet state. The prepared UHA-based membranes with different GO loading ratios (10, 20, 30, 40, 50, and 60 mg) in addition to the blank membrane (Fig. S7, cf. ESM) were tested. The prepared 50 mg GO/UHA membrane showed the highest obtained water flux of 42 ± 2 LMH, which is 3.3 times higher than the pristine 0 mg GO/UHA membrane (Fig. 11(b)).

The better FO membrane performance was achieved by different factors: (1) reduction of the membrane thickness that greatly reduced the internal concentration polarization (ICP) phenomenon and increased the flux due to a reduction of the structural parameters of the substrate layer [24,38], (2) increase of the surface area of the membrane interface layers that resulted from inner and interconnected pores or the high roughness of the membrane surface due to the nanofibrous formation [39−41], and (3) improvement of the osmotic pressure gradient on both sides of the FO membrane for effective osmotic driving force [42−45]. The improved water flux of the 50 mg GO/UHA membrane compared to other membranes is mainly attributed to its lower thickness (319 μm) and the large surface area that resulted from the formed nanofibrous on the surface as indicated by the SEM images and contact angle of 145°. Although the 60 mg GO/UHA membrane has a comparable thickness of 341 μm, it showed a lower water flux of 9.3 LMH. This reduction in water flux may be attributed to its

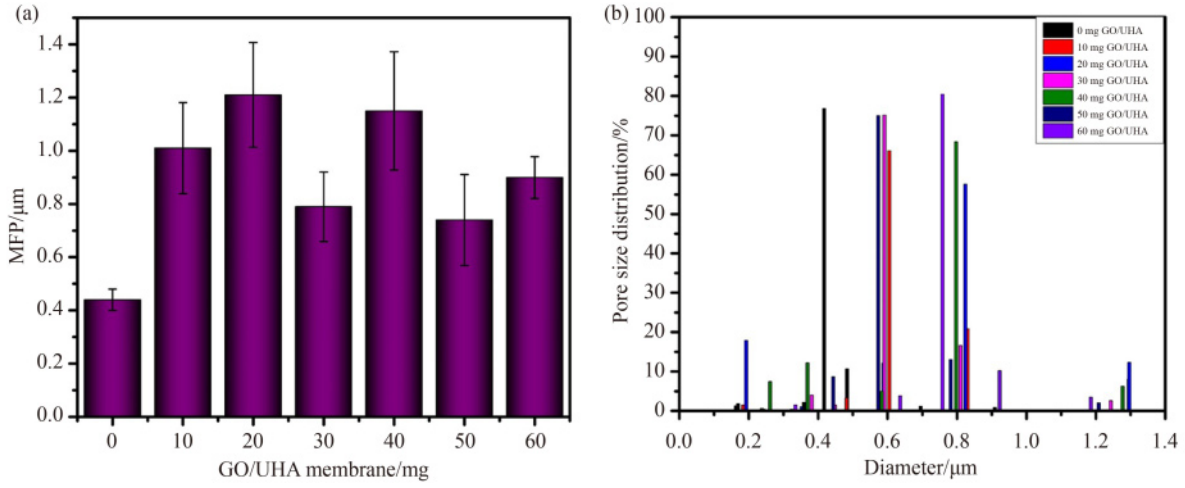

Fig. 10 The pore size flow distribution analysis of the GO/UHA membranes. (a) The MFP, and (b) the pore size flow distribution.

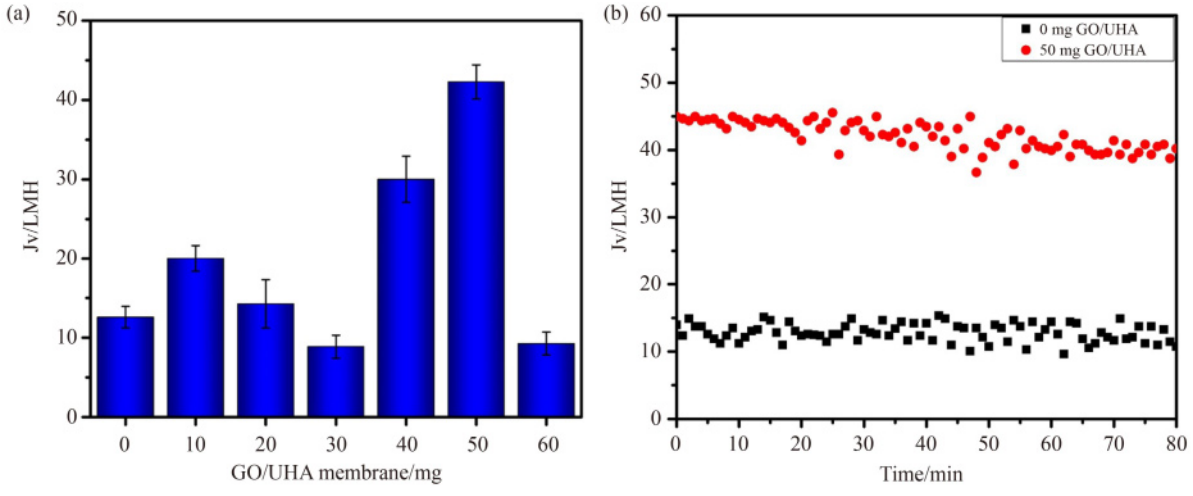

Fig. 11 Performance evaluation of the GO/UHA membranes. (a) Water flux, and (b) comparison of water flux of 0 mg GO/UHA membrane and 50 mg GO/UHA membrane.

superhydrophobic surface with a water contact angle of 150° due to the high conversion rate of GO to rGO as shown in FTIR (Fig. 6) leading to an increase in the ICP.

Figure 12 shows the reverse salt flux of the prepared GO/UHA membranes. The reverse salt flux decreased from 118.4 gMH for the 40 mg GO/UHA membrane to 67 gMH for the 50 mg GO/UHA membrane. The success indicator of FO membrane performance resulting in the low reverse salt flux along with high osmotic water flux [46].

A number of new strategies to improve membrane performance and development are now being examined in the context of developing water treatment technologies. The use of inorganic nanowire materials to fabricate FO membranes can improve separation performance and develop new functionalities, which nanowire materials provide. Compared to conventional polymeric FO membranes, the inorganic hybrid nanowire composite membranes have a significantly higher water flux, good mechanical strength, fire resistance, thermal stability, selectivity, and biocompatible properties [47]. To reduce ICP, minimize fouling, and overcome the tradeoff effect, the incorporation of nanowires into FO membranes aims to achieve optimal structures. The interactions between the nanowire materials, the molecular bonds present in GO, and the functional groups present in GO are the main reasons for the improved performance. To meet the requirements of specific application areas, it is therefore possible that an innovative nanoporous composite FO membrane with complete functionality would be substituted for conventional fluorinated organic membranes. Table 2 summarizes the utilized nanomaterials composed of the performance of FO membranes.

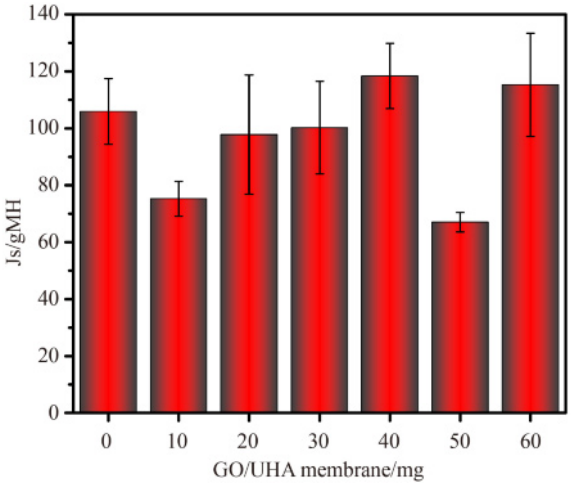

Fig. 12 Reverse salt flux of the GO/UHA membranes.

4 Conclusions

A novel kind of sustainable inorganic-based FO membrane for freshwater generation has been developed. The developed membranes were tested by Sterlitech FO module for performance evaluation using deionized water as a feed solution and 2.0 mol·L^{-1} NaCl as a draw solution. Different ratios of GO with 0, 10, 20, 30, 40, 50, and 60 mg were mixed with the solvothermal-prepared hydroxyapatite nanowire (UHA) to fabricate the GO/UHA membranes. The obtained membranes showed different pore size ranging from 0.44 μm of the pristine membrane (0 mg GO/UHA) to 1.21 μm of the 20 mg GO/UHA membrane. The homogeneous and uniform pore size flow distribution was noticed for the 50 mg GO/UHA membranes where 75% achieved at 0.59 μm, while 13.1% and 8.7% achieved at 0.8, and 0.46 μm, respectively. The improved water flux of 42.28 LMH and reverse salt flux of 67.013 gMH was noticed for the 50 mg GO/UHA membrane. The obtained results showed that the best mixed design ratios of GO (2D) and UHA (nanowires of 1D) is the 50 mg of GO that dopped to the UHA achieving the optimized hydrogen bonding interactions with a uniform pore size distribution and effective interconnective pores and microchannel. This novel kind of membrane still need more intensive investigation of freshwater generation from different water and wastewater resources. The membrane expects to resist thermal, chemical and mechanical operating wastewater treatment conditions, in addition to promising

Table 2 Comparison of nanomaterials composed membranes applied in FO

No.	Materials[a)]	Membrane	Draw solution	Feed solution	Water flux/LMH	Reverse salt flux/gMH	Ref.
1	SiO_2/PS	FO	Deionized water	2 mol·L^{-1} NaCl	22.3	21	[48]
2	HAP/CA	FO	Deionized water	2 mol·L^{-1} NaCl	4.5 to 7.5	15–120	[49]
3	SiO_2/TFN	FO	Deionized water	2 mol·L^{-1} NaCl	36	6.0	[50]
4	GO/PES	FO	Deionized water	2 mol·L^{-1} NaCl	41.4	120	[23]
5	TiO_2/PS	FO	Deionized water	2 mol·L^{-1} NaCl	33	20	[51]
6	HNTs/PS	FO	10 Mm NaCl	2 mol·L^{-1} NaCl	41	17	[52]
7	Boehmite/CA/CTA	FO	10 Mm NaCl	2 mol·L^{-1} NaCl	23	7.0	[53]
8	GO/UHA	FO	Deionized water	2 mol·L^{-1} NaCl	42.28	65	This work

a) PS: polysulfone; HAP: hydroxyapatite; CA: cellulose acetate; PES: polyethersulfone; HNTs: Hallosite nanotubes; CTA: cellulose triacetate.

applications of photothermal evaporation, membrane distillation and photothermal membrane distillations.

Competing Interests The authors declare that they have no competing interests.

Acknowledgements This work has been carried out within the received fund through the CNR-ASRT (Italy-Egypt) 2022–2023 international Exchanges (project ID: 18775), and the Science and Technology Development Fund (STDF), projects ID 41528 and 43224. We thank Prof. David A. Ladner (Clemson University, USA) for his assistance in SEM surface morphology and cross-section investigation of the membranes.

Electronic Supplementary Material Supplementary material is available in the online version of this article at https://doi.org/10.1007/s11705-024-2450-0 and is accessible for authorized users.

Funding Note Open access funding provided by The Science, Technology & Innovation Funding Authority (STDF) in cooperation with The Egyptian Knowledge Bank (EKB).

References

1. Nunes S P, Culfaz-Emecen P Z, Ramon G Z, Visser T, Koops G H, Jin W, Ulbricht M. Thinking the future of membranes: perspectives for advanced and new membrane materials and manufacturing processes. Journal of Membrane Science, 2020, 598: 117761
2. Keyikoglu R, Karatas O, Rezania H, Kobya M, Vatanpour V, Khataee A. A review on treatment of membrane concentrates generated from landfill leachate treatment processes. Separation and Purification Technology, 2021, 259: 118182
3. Yadav P, Ismail N, Essalhi M, Tysklind M, Athanassiadis D, Tavajohi N. Assessment of the environmental impact of polymeric membrane production. Journal of Membrane Science, 2021, 622: 118987
4. Ismail N, Pan J, Rahmati M, Wang Q, Bouyer D, Khayet M, Cui Z, Tavajohi N. Non-ionic deep eutectic solvents for membrane formation. Journal of Membrane Science, 2022, 646: 120238
5. Benfer S, Popp U, Richter H, Siewert C, Tomandl G. Development and characterization of ceramic nanofiltration membranes. Separation and Purification Technology, 2001, 22–23(1–2): 231–237
6. Kayvani Fard A, McKay G, Buekenhoudt A, Al Sulaiti H, Motmans F, Khraisheh M, Atieh M. Inorganic membranes: preparation and application for water treatment and desalination. Materials, 2018, 11(1): 74
7. Verweij H. Inorganic membranes. Current Opinion in Chemical Engineering, 2012, 1(2): 156–162
8. Chung T S, Jiang L Y, Li Y, Kulprathipanja S. Mixed matrix membranes (MMMs) comprising organic polymers with dispersed inorganic fillers for gas separation. Progress in Polymer Science, 2007, 32(4): 483–507
9. Sanchez C, Belleville P, Popall M, Nicole L. Applications of advanced hybrid organic-inorganic nanomaterials: from laboratory to market. Chemical Society Reviews, 2011, 40(2): 696–753
10. Lu B Q, Zhu Y J, Chen F. Highly flexible and nonflammable inorganic hydroxyapatite paper. Chemistry, 2014, 20(5): 1242–1246
11. Shao Y T, Zhu Y J, Dong L Y, Zhang Q Q. A new kind of nanocomposite Xuan paper comprising ultralong hydroxyapatite nanowires and cellulose fibers with a unique ink wetting performance. RSC Advances, 2019, 9(69): 40750–40757
12. Zhang Q Q, Zhu Y J, Wu J, Shao Y T, Dong L Y. A new kind of filter paper comprising ultralong hydroxyapatite nanowires and double metal oxide nanosheets for high-performance dye separation. Journal of Colloid and Interface Science, 2020, 575: 78–87
13. Qin D D, Zhu Y J, Chen F F, Yang R L, Xiong Z C. Self-floating aerogel composed of carbon nanotubes and ultralong hydroxyapatite nanowires for highly efficient solar energy-assisted water purification. Carbon, 2019, 150: 233–243
14. Eide E B. Global Risks 2015. 10th ed. World Economic Forum, 2015
15. Mekonnen M M, Hoekstra A Y. Four billion people facing severe water scarcity. Science Advances, 2016, 2(2): e1500323
16. Cath T Y, Childress A E, Elimelech M. Forward osmosis: principles, applications, and recent developments. Journal of Membrane Science, 2006, 281(1-2): 70–87
17. Aliyev E, Filiz V, Khan M M, Lee Y J, Abetz C, Abetz V. Structural characterization of graphene oxide: surface functional groups and fractionated oxidative debris. Nanomaterials, 2019, 9(8): 1180
18. Zhang L, Lu Y, Liu Y L, Li M, Zhao H Y, Hou L A. High flux MWCNTs-interlinked GO hybrid membranes survived in cross-flow filtration for the treatment of strontium-containing wastewater. Journal of Hazardous Materials, 2016, 320: 187–193
19. Jiang D, Cooper V R, Dai S. Porous graphene as the ultimate membrane for gas separation. Nano Letters, 2009, 9(12): 4019–4024
20. Xiong Z C, Yang R L, Zhu Y J, Chen F F, Dong L Y. Flexible hydroxyapatite ultralong nanowire-based paper for highly efficient and multifunctional air filtration. Journal of Materials Chemistry. A, Materials for Energy and Sustainability, 2017, 5(33): 17482–17491
21. Li H, Zhu Y, Jiang Y, Yu Y, Chen F, Dong L, Wu J. Hierarchical assembly of monodisperse hydroxyapatite nanowires and construction of high-strength fire-resistant inorganic paper with high-temperature flexibility. Chem Nano Mat: Chemistry of Nanomaterials for Energy, Biology and More, 2017, 3(4): 259–268

22. Wang Y, Ou R, Wang H, Xu T. Graphene oxide modified graphitic carbon nitride as a modifier for thin film composite forward osmosis membrane. Journal of Membrane Science, 2015, 475: 281–289
23. Hummers W S Jr, Offeman R E. Preparation of graphitic oxide. Journal of the American Chemical Society, 1958, 80(6): 1339
24. Song X, Zhang Y, Abdel-Ghafar H M, Abdel-Aal E A, Huang M, Gul S, Jiang H. Polyamide membrane with an ultrathin GO interlayer on macroporous substrate for minimizing internal concentration polarization in forward osmosis. Chemical Engineering Journal, 2021, 412: 128607
25. Duong P H H, Zuo J, Chung T S. Highly crosslinked layer-by-layer polyelectrolyte FO membranes: understanding effects of salt concentration and deposition time on FO performance. Journal of Membrane Science, 2013, 427: 411–421
26. Zhang Q Q, Zhu Y J, Wu J, Dong L Y. Nanofiltration filter paper based on ultralong hydroxyapatite nanowires and cellulose fibers/nanofibers. ACS Sustainable Chemistry & Engineering, 2019, 7(20): 17198–17209
27. Qiao X, Liao S, You C, Chen R. Phosphorus and nitrogen dual doped and simultaneously reduced graphene oxide with high surface area as efficient metal-free electrocatalyst for oxygen reduction. Catalysts, 2015, 5(2): 981–991
28. Flora B, Kumar R, Tiwari P, Kumar A, Ruokolainen J, Narasimhan A K, Kesari K K, Gupta P K, Singh A. Development of chemically synthesized hydroxyapatite composite with reduced graphene oxide for enhanced mechanical properties. Journal of the Mechanical Behavior of Biomedical Materials, 2023, 142: 105845
29. Ceniceros-Reyes M A, Marín-Hernández K S, Sierra U, Saucedo-Salazar E M, Mendoza-Resendez R, Luna C, Hernández-Belmares P J, Rodríguez-Fernández O S, Fernández-Tavizón S, Hernández-Hernández E, et al. Reduction of graphene oxide by *in-situ* heating experiments in the transmission electron microscope. Surfaces and Interfaces, 2022, 35: 102448
30. Wang J, Yu Z, Xiao X, Chen Z, Huang J, Liu Y. Xiao X, Chen Z, Huang J, Liu Y. A novel hydroxyapatite super-hydrophilic membrane for efficient separation of oil-water emulsions, desalting and removal of metal ions. Desalination, 2023, 565: 116864
31. Xiong Z C, Zhu Y J, Chen F F, Sun T W, Shen Y Q. One-step synthesis of silver nanoparticle-decorated hydroxyapatite nanowires for the construction of highly flexible free-standing paper with high antibacterial activity. Chemistry, 2016, 22(32): 11224–11231
32. Xiong Z C, Zhu Y J, Qin D D, Yang R L. Flexible salt-rejecting photothermal paper based on reduced graphene oxide and hydroxyapatite nanowires for high-efficiency solar energy-driven vapor generation and stable desalination. ACS Applied Materials & Interfaces, 2020, 12(29): 32556–32565
33. Lu B Q, Zhu Y J, Chen F. Highly flexible and nonflammable inorganic hydroxyapatite paper. Chemistry, 2014, 20(5): 1242–1246
34. Atchudan R, Perumal S, Joo J, Lee Y R. Synthesis and characterization of monodispersed spherical calcium oxide and calcium carbonate nanoparticles via simple pyrolysis. Nanomaterials, 2022, 12(14): 2424
35. Bharath G, Latha B S, Alsharaeh E H, Prakash P, Ponpandian N. Enhanced hydroxyapatite nanorods formation on graphene oxide nanocomposite as a potential candidate for protein adsorption, pH controlled release and an effective drug delivery platform for cancer therapy. Analytical Methods, 2017, 9(2): 240–252
36. Chen F F, Zhu Y J, Zhang Y G, Yang R L, Yu H P, Qin D D, Xiong Z C. Portable and writable photoluminescent chalk for on-site information protection on arbitrary substrates. Chemical Engineering Journal, 2019, 369: 766–774
37. Huang Z, Gengenbach T, Tian J, Shen W, Garnier G. The role of polyaminoamide-epichlorohydrin (PAE) on antibody longevity in bioactive paper. Colloids and Surfaces. B, Biointerfaces, 2017, 158: 197–202
38. Niu F, Huang M, Cai T, Meng L. Effect of membrane thickness on properties of FO membranes with nanofibrous substrate. IOP Conference Series. Earth and Environmental Science, 2018, 170(5): 052005
39. Song X, Dong W, Zhang Y, Abdel-Ghafar H M, Toghan A, Jiang H. Coupling solar-driven interfacial evaporation with forward osmosis for continuous water treatment. Exploration, 2022, 2(4): 20220054
40. Zhou Z, Hu Y, Boo C, Liu Z, Li J, Deng L, An X. High-performance thin-film composite membrane with an ultrathin spray-coated carbon nanotube interlayer. Environmental Science & Technology Letters, 2018, 5(5): 243–248
41. Song X, Zhou Q, Zhang T, Xu H, Wang Z. Pressure-assisted preparation of graphene oxide quantum dot-incorporated reverse osmosis membranes: antifouling and chlorine resistance potentials. Journal of Materials Chemistry. A, Materials for Energy and Sustainability, 2016, 4(43): 16896–16905
42. Wang Q, Zhou Z, Li J, Tang Q, Hu Y. Modeling and measurement of temperature and draw solution concentration induced water flux increment efficiencies in the forward osmosis membrane process. Desalination, 2019, 452: 75–86
43. Huang J, Xiong S, Long Q, Shen L, Wang Y. Evaluation of food additive sodium phytate as a novel draw solute for forward osmosis. Desalination, 2018, 448: 87–92
44. Zhao W, Liu H, Liu Y, Jian M, Gao L, Wang H, Zhang X. Thin-film nanocomposite forward-osmosis membranes on hydrophilic microfiltration support with an intermediate layer of graphene oxide and multiwall carbon nanotube. ACS Applied Materials & Interfaces, 2018, 10(40): 34464–34474
45. Han J C, Wang S F, Deng R, Wu Q Y. Polydopamine/imogolite nanotubes (PDA/INTs) interlayer modulated thin film composite forward osmosis membrane for minimizing internal concentration polarization. Chinese Journal of Polymer Science, 2022, 40(10): 1233–1241
46. Alfahel R, Azzam R S, Hafiz M, Hawari A H, Pandey R P, Mahmoud K A, Hassan M K, Elzatahry A A. Fabrication of fouling-resistant $Ti_3C_2T_x$ (MXene)/cellulose acetate nanocomposite membrane for forward osmosis application. Journal of Water Process Engineering, 2020, 38: 101551
47. Liu G, Han K, Ye H, Zhu C, Gao Y, Liu Y, Zhou Y. Graphene oxide/triethanolamine modified titanate nanowires as photocatalytic membrane for water treatment. Chemical

Engineering Journal, 2017, 320: 74–80

48. Huang Y, Jin H, Yu P, Luo Y. Polyamide thin-film composite membrane based on nano-silica modified polysulfone microporous support layer for forward osmosis. Desalination and Water Treatment, 2016, 57(43): 20177–20187
49. Ohland A L, Salim V M M, Borges C P. Plasma functionalized hydroxyapatite incorporated in membranes for improved performance of osmotic processes. Desalination, 2019, 452: 87–93
50. Niksefat N, Jahanshahi M, Rahimpour A. The effect of SiO_2 nanoparticles on morphology and performance of thin film composite membranes for forward osmosis application. Desalination, 2014, 343: 140–146
51. Emadzadeh D, Lau W J, Matsuura T, Ismail A F, Rahbari-Sisakht M. Synthesis and characterization of thin film nanocomposite forward osmosis membrane with hydrophilic nanocomposite support to reduce internal concentration polarization. Journal of Membrane Science, 2014, 449: 74–85
52. Ghanbari M, Emadzadeh D, Lau W J, Lai S O, Matsuura T, Ismail A F. Synthesis and characterization of novel thin film nanocomposite (TFN) membranes embedded with halloysite nanotubes (HNTs) for water desalination. Desalination, 2015, 358: 33–41
53. Zirehpour A, Rahimpour A, Seyedpour F, Jahanshahi M. Developing new CTA/CA-based membrane containing hydrophilic nanoparticles to enhance the forward osmosis desalination. Desalination, 2015, 371: 46–57